Article

Implementation of Large Area Diffractive Lens Using Multiple Sub-Aperture Diffractive Lenses and Computational Reconstruction

Shivasubramanian Gopinath[1,†], Praveen Periysamy Angamuthu[1,†], Tauno Kahro[1,†], Andrei Bleahu[1], Francis Gracy Arockiaraj[1,2], Daniel Smith[3], Soon Hock Ng[3], Saulius Juodkazis[3,4], Kaupo Kukli[1], Aile Tamm[1] and Vijayakumar Anand[1,3,*]

[1] Institute of Physics, University of Tartu, W. Ostwaldi str. 1, 50411 Tartu, Estonia
[2] PG and Research Department of Physics, The American College, Madurai 625002, India
[3] Optical Sciences Center, Swinburne University of Technology, Melbourne 3122, Australia
[4] Tokyo Tech World Research Hub Initiative (WRHI), School of Materials and Chemical Technology, Tokyo Institute of Technology, 2-12-1, Ookayama, Meguro-ku, Tokyo 152-8550, Japan
* Correspondence: vijayakumar.anand@ut.ee
† The authors contributed equally to this work

Abstract: Direct imaging systems that create an image of an object directly on the sensor in a single step are prone to many constraints as a perfect image is required to be recorded within this step. In designing high resolution direct imaging systems with a diffractive lens, the outermost zone width either reaches the lithography limit or the diffraction limit itself imposing challenges in fabrication. However, if the imaging mode is switched to an indirect one consisting of multiple steps to complete imaging, then different possibilities open up. One such methods is the widely used indirect imaging method with Golay configuration telescopes. In this study, a Golay-like configuration has been adapted to realize a large area diffractive lens with three sub-aperture diffractive lenses. The sub-aperture diffractive lenses are not required to collect light and focus them to a single point as in a direct imaging system but to focus independently on different points within the sensor area. This approach of Large Area Diffractive lens with Integrated Sub-Apertures (LADISA) relaxes the fabrication constraints and allows the sub-aperture diffractive elements to have a larger outermost zone width and smaller area. The diffractive sub-apertures were manufactured using photolithography. The fabricated diffractive element has been implemented in indirect imaging mode using non-linear reconstruction and Lucy-Richardson-Rosen algorithm with synthesized point spread functions. The computational optical experiments revealed an improved optical and computational imaging resolutions compared to previous studies.

Keywords: diffractive lens; imaging; Lucy-Richardson-Rosen algorithm; holography; incoherent imaging; telescope; photolithography; computational imaging

1. Introduction

Imaging systems and components have occupied a significant part of our day-to-day life, starting from our built-in imager - eye to all vision enhancement imaging systems and components such as microscopes, telescopes, web camera, smart phone camera, etc. However, most of the available imaging systems as such as the ones above fall predominantly into the direct imaging category. A direct imaging system uses a conventional imaging mode consisting of a single step – the image of an object is directly formed by a lens on the sensor [1]. An alternative method for imaging is by indirect imaging mode, which, as the name suggests involve multiple steps to complete the imaging process. Some examples of indirect imaging method are digital holography [2] and coded aperture imaging [3], both can be used with coherent as well as incoherent light sources. Coherent light sources are often limited to lab environments unlike incoherent

Preprints (www.preprints.org) | NOT PEER-REVIEWED | Posted: 15 November 2022 doi:10.20944/preprints202211.0281.v1

ones which have a broad applicability. In incoherent digital holography (IDH), the light from an object is split into two, differently modulated and interfered to create a hologram which is processed in the computer to reconstruct the 3D object information [4,5]. Hence, IDH require two beam interference resulting in complicated optical configurations, and bulky, and heavy optical systems. Some notable optical configurations of IDH are rotational shearing interferometer [6,7], multiple view point projection methods [8,9], conoscopic holography [10,11], optical scanning holography [12, 13], Fresnel incoherent correlation holography [14, 15] and coded aperture correlation holography (COACH) [16]. As it appears from the above discussion, indirect imaging requires a complicated system and the imaging procedure involves multiple steps in comparison to conventional imaging. However, the significantly higher density of information made available in 3D within few camera recordings in comparison to 2D information captured using direct imaging methods, justifies the experimental requirements of IDH.

Like holography, coded aperture imaging (CAI) methods as well exhibit advantages in comparison to direct imaging methods. Pinhole imaging system can be considered as the oldest coded direct imaging system. However, imaging using pinhole has significantly low light throughput and therefore not suitable for many applications. The history and development of CAI methods in indirect mode are interesting [17-20]. The main motivation for the beginning of research in CAI was the lack of availability of technology to manufacture lenses for non-visible regions of the electromagnetic spectrum such as X-rays and Gamma rays [17, 18]. Dicke and Ables employed a random pinhole array to scatter light from the object and reconstructed it numerically by processing it with the pre-recorded or synthesized point spread function (PSF). Later, CAI was extended to 3D imaging in 2D space and spectrum (x,y,λ), unlike holography which can record object information in 3D space (x,y,z). Recently, CAI met holography when the COACH technique was developed. In COACH, the recording method involved two beam interference like holography but the reconstruction was similar to CAI involving a cross-correlation with the PSF. Later, COACH evolved into I-COACH when the two beam interference was found redundant as the 4D information of the object (x,y,z,λ) was found to be contained in the light scattered from a coded phase mask if the spatial (z) and spectral (λ) PSFs are known [21-24]. From a single camera shot, the entire 4D information of the object can be reconstructed.

Golay-type synthetic aperture configuration for telescopes is a powerful approach to achieve super-resolution [25, 26]. In Golay-type synthetic aperture telescopes, a single aperture was replaced by multiple sparse sub-apertures which reduces the cost and complications associated with manufacturing large area lenses and mirrors [27]. In [27], a Weiner type deconvolution method was implemented to improve the raw Golay image [28]. Different types of deconvolution methods have been applied for reconstructing the object information recorded in Golay-type imaging systems [29,30]. In this study, the indirect imaging concepts and the optical configuration inspired by Golay-type imaging systems have been integrated to solve one fundamental problem associated with the design and manufacturing of a large area diffractive lenses [31].

Design and manufacturing of large area diffractive lenses for any imaging system - telescope, microscope, projection or display and holography systems, are challenging for the following reasons. The radius of the zones of a diffractive lens is given as $r_n \sim \sqrt{nf\lambda}$, where n is an integer which is the order of the half-period zone, f is the focal length and λ is the wavelength. The thickness of the n^{th} zone is therefore given as $\Delta_n \sim \left\{\sqrt{nf\lambda} - \sqrt{(n-1)f\lambda}\right\}$, which can be simplified as $\Delta_n \sim \left[\sqrt{f\lambda}\left\{\sqrt{n} - \sqrt{(n-1)}\right\}\right]$. As seen from this expression, as n increases Δ_n decreases and for very large values of n, Δ_n reaches significantly low values. Consequently, the fabrication of the outermost areas of a diffractive lens is challenging as these areas have features that are either sub-lithography limit or even sub-diffraction limit with polarization sensitivity [32, 33].

One of the widely used solutions to solve this problem once the lithography or diffraction limit is reached is to maintain the same period after this cut-off radius i.e.,

Preprints (www.preprints.org) | NOT PEER-REVIEWED | Posted: 15 November 2022 doi:10.20944/preprints202211.0281.v1

$_n = \left[\sqrt{f\lambda}\left\{\sqrt{m} - \sqrt{(m-1)}\right\}\right]$ for $n \geq m$, where n=m is the cut-off radius, when $_n$ reaches the lithography limit $_l$ [34]. In general, the above approximation does not affect the behavior of diffractive lens as the variation of r_n with respect to n is non-linear near the central part and nearly linear in the outermost part. However, in high numerical aperture (NA) lenses, it is possible that the lithography limit is reached within the non-linear region of r_n vs n variation. In such high NA cases, the above approximation results in spherical aberrations [35]. The consequences worsen if the diffractive lens is needed in finite conjugate mode instead of infinite conjugate mode [35]. The concept figure of the problem is shown in Figure 1.

A diffractive lens is designed for infinite conjugate mode with f = 20 mm, λ = 0.65 μm, and 100 number of half period zones. The above number of zones were selected assuming a scenario of printing diffractive lens in inkjet printer which has ~1200 dots per inch with a pixel size of about 20 μm. Three scenarios are considered in the case of a high NA diffractive lens: (a) ideal diffractive lens with all the zones fabricated according to the theory, (b) diffractive lens fabricated according to the theory until the lithography limit (~ 20 μm with inkjet printer) and constant zone width maintained henceforth and (c) diffractive lens fabricated only until the lithography limit. The images of the binary versions of accurate diffractive lens, approximate diffractive lens and low NA lens are shown in Figures 1(b)-1(d) respectively. The PSF of the above three cases Figures 1(b)-1(d) are shown in Figures 1(e) – 1(g) respectively. A test object 'camera man' was imaged and the imaging results for the cases Figures 1(b)-1(d) are shown in Figures 1(h)-1(j) respectively. The imaging process was simulated using a binary phase version (0, π) of diffractive lens to avoid the unmodulated light which may cause difficulty in comparing the performances of the three diffractive lenses. As seen from the imaging results, the existing approximation approach surely improved the resolution of imaging but is not as high as the accurate diffractive lens. However, if imaging is not the focus but only light collection, then there is not difference between an approximate and accurate diffractive lens. The second challenge in manufacturing large area diffractive lenses is the memory size of the CAD files. In many cases [35], the source files for the CAD files are image files generated directly using computational simulation in software like MATLAB and converted into CAD files using conversion software such as 'LinkCAD' to avoid manually creating zone by zone of thousands of zones.

In this study, Golay-type configuration inspired imaging system and indirect imaging concepts have been integrated to redefine the imaging problem with a diffractive lens. When a diffractive lens is designed, the radii of the zones were calculated such that the light from every radial zone will constructively interfere at a single point. This requirement shrinks the widths of the zones in the outermost areas of the diffractive lens as higher diffraction angles are required from zones far away from the optical center. Applying Golay-type configuration, the above condition can be relaxed. Since the image is captured by an image sensor, the condition for imaging is redefined to collect and focus light within the image sensor's active area instead of a single point. This new condition allows to design sub-aperture diffractive lenses with a low NA and integrate them into a larger diffractive lens. This new diffractive lens can collect all the spatial frequencies within the full aperture and accumulate them within the sensor area. This new diffractive lens is called Large Area Diffractive lens with Integrated Sub-Apertures (LADISA). But the recorded image appears blurred due to the overlap of several low-resolution images of the object. Using the indirect imaging concepts, the recorded intensity distribution can be reconstructed using computational reconstruction methods into a super-resolution image. This super-resolution is achieved in comparison to a single sub-aperture or currently available unsuccessful methods. The above approach also solves the problem with large memory sizes of CAD designs as the individual file sizes of sub-aperture diffractive lenses are significantly smaller the memory size of a large area diffractive lens. Unlike I-COACH and CAI, in this study, it is not necessary to record a PSF as it can be

Preprints (www.preprints.org) | NOT PEER-REVIEWED | Posted: 15 November 2022 doi:10.20944/preprints202211.0281.v1

easily synthesized from the object intensity distribution which makes this approach non-invasive.

The manuscript consists of five sections. In the next section on methodology, the design of LADISA and the imaging process is described. The simulation studies are presented in the third section. The fabrication procedure is presented in the fourth section. The experimental results are presented in the fifth section. The final section presents the summary, conclusion and future perspectives of the study.

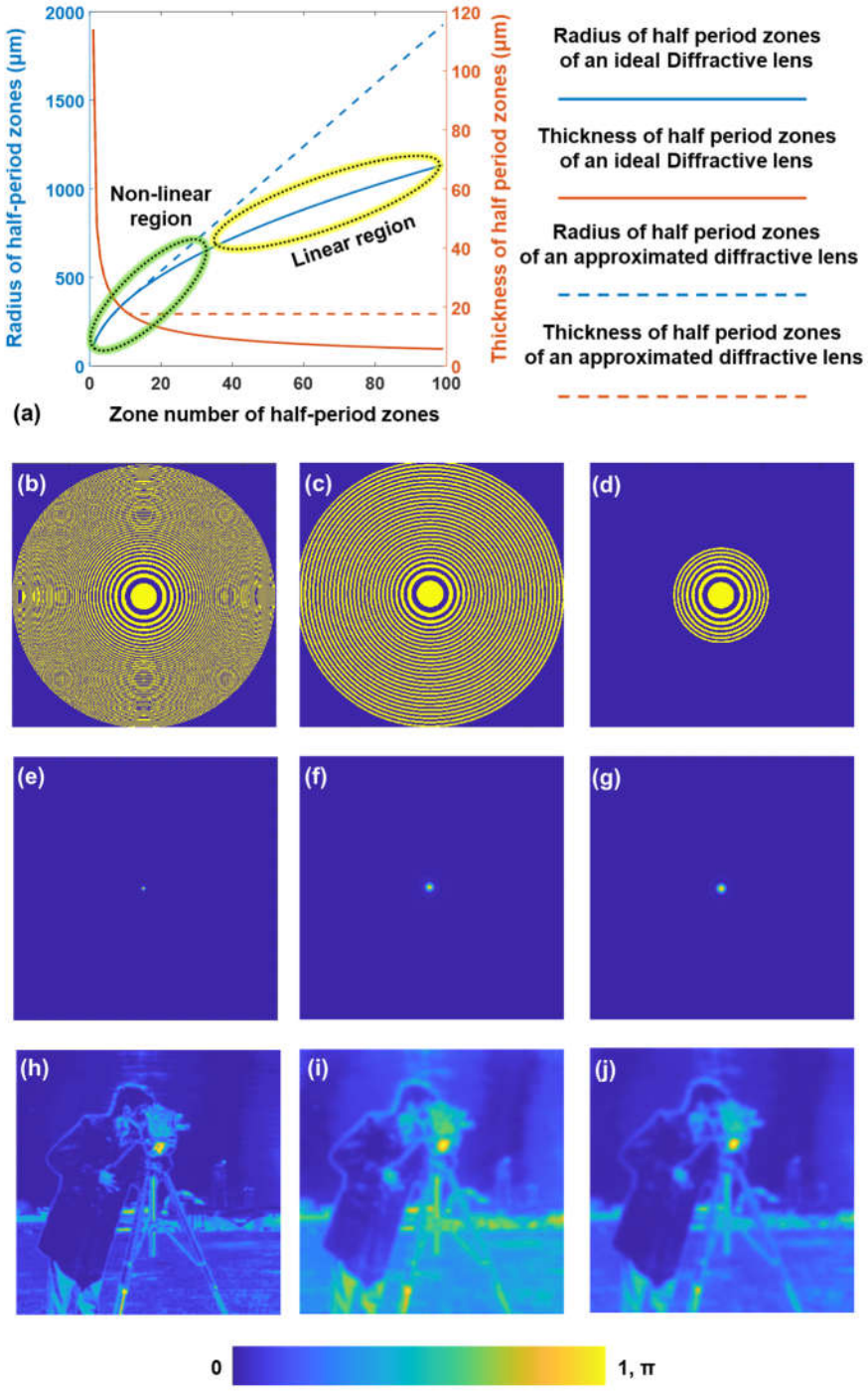

Figure 1. (a) Plot of radius and thickness of zones of an accurate and approximate diffractive lens. Phase image of (b) accurate diffractive lens, (c) approximate diffractive lens and (d) diffractive lens within the lithography limit. PSF of (e) accurate diffractive lens, (f) approximate diffractive lens and (g) diffractive lens within the lithography limit. Imaging results of a test object obtained using (h)

Preprints (www.preprints.org) | NOT PEER-REVIEWED | Posted: 15 November 2022 doi:10.20944/preprints202211.0281.v1

accurate diffractive lens, (i) approximate diffractive lens and (j) diffractive lens within the lithography limit.

2. Methodology

The optical configuration of the imaging system is shown in Figure 2. Spatially incoherent light from a distant object is incident on the LADISA with three sub-apertures. Several low-resolution images of the objects were formed on the sensor. The diffractive element LADISA is composed of three diffractive lenses approximated by quadratic phase functions whose phase function is given as $\Psi_{LADISA} = \sum_{a=1}^{3} \exp\left[-j\pi {R_a}^2/(\lambda f)\right] \times P_a \times \exp\left[j\left(\theta_{x_a} + \theta_{y_a}\right)\right]$, where R_a is the radial coordinate $R_a = \sqrt{(x - x_a)^2 + (y - y_a)^2}$, $P_a = \begin{cases} 1, & R_a < r_s \\ 0, & elsewhere' \end{cases}$ where r_s is the radius of the sub-aperture, θ_{x_a} and θ_{y_a} are the angles of the linear phases along the x and y directions and '×' represents element-wise product. The distance between the centers of any two sub-apertures is greater than twice the value of r_s. Since the object distance z_s is assumed very large, the PSF can be approximated as

$$I_{PSF} = \left|\sum_{a=1}^{3} \exp\left[-j\pi {R_a}^2/(\lambda f)\right] \times P_a \times \exp\left[j\left(\theta_{x_a} + \theta_{y_a}\right)\right] \otimes \exp[j\pi R^2/(\lambda z_h)]\right|^2, \quad (1)$$

where, '⊗' is a 2D convolutional operator and $R = \sqrt{x^2 + y^2}$. It can be seen that when $z_h = f$, the above expression reduces to the square of the sum of Fourier transforms of the aperture function and the linear phases given as

$$I_{PSF} = \left|\Im\left[\sum_{a=1}^{3}\left\{\exp\left[j\left(\theta_{x_a} + \theta_{y_a}\right)\right] \times P_a\right\}\right]\right|^2, \quad (2)$$

where '$\Im$' is the Fourier transform operator. Since, the design has been made such that the three image spots do not overlap, using the linearity property of Fourier transform, the Eq. (2) can be modified also as sums of intensity distributions from individual apertures. The above Fourier transform operation on three apertures and linear phases generate Airy patterns each with a size of $1.22\lambda f/2r_s$ at three different locations in the sensor plane. The size of the Airy pattern obtained by the full aperture is $>1.22\lambda f/4r_s$. The individual spot sizes are larger than the spot size obtained from the full aperture but they have the information of higher spatial frequencies which can be retrieved using a suitable computational reconstruction method.

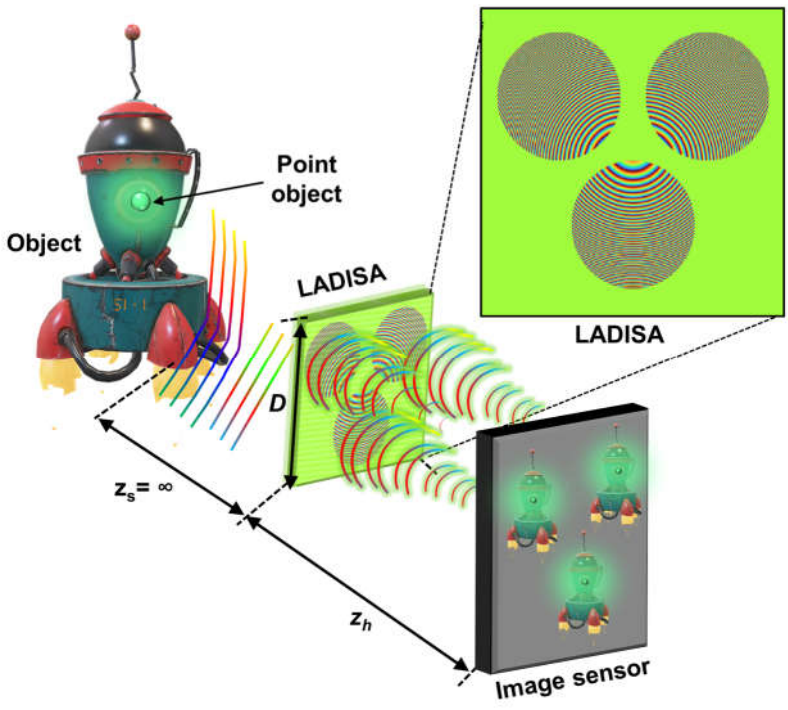

Figure 2. Optical configuration of the Golay-type diffractive imaging system consisting of LADISA with three sub-apertures.

Preprints (www.preprints.org) | NOT PEER-REVIEWED | Posted: 15 November 2022 doi:10.20944/preprints202211.0281.v1

Considering a 2D object O at a large distance from the LADISA similar to the telescopic Golay-configuration, the object intensity distribution is given as $I_O = O \otimes I_{\mathrm{PSF}}$. Now the challenge is to extract the image of the object O, from I_O and I_{PSF}. This can be achieved using different types of correlation such as matched filter, phase-only filter [36], Wiener filter or inverse filter [37] and non-linear reconstruction (NLR) method [38]. The NLR approach is a generalized correlation method in which matched, phase-only, Wiener filter are only special cases. The reconstructed image using NLR is given as

$$I_R = \mathcal{F}^{-1}\left\{\left|\tilde{I}_{PSF}\right|^{\alpha}\exp[j\cdot\arg(\tilde{I}_{PSF})]\left|\tilde{I}_O\right|^{\beta}\exp[-j\cdot\arg(\tilde{I}_O)]\right\}, \quad (3)$$

where α and β are varied between -1 to 1 until a minimum background noise was obtained. When α = 1, and β = 1, it is a matched filter, when α = 0, and β = 1, it is a phase-only filter, when α = -1, and β = 1, it is a Wiener filter. It has been well-established by various studies that NLR performs significantly better than the other filters [28]. While all the above methods use correlation approach, an alternative method to reconstruct the object information is the Lucy-Richardson algorithm (LRA) which estimates the maximum likelihood solution iteratively [39, 40]. Recently, a novel computational reconstruction method called the Lucy-Richardson-Rosen algorithm (LRRA) was developed by integrating LRA and NLR [41]. The schematic of LRRA is shown in Figure 3. The LRA consists of a forward convolution between the approximate solution and the PSF and a backward correlation between the PSF and the ratio between I_O and the estimated solution. This ratio is multiplied to the previous solution and this process is continued until an optimal solution is obtained. In LRRA, the backward correlation (matched filter) is replaced by NLR which not only improved the estimation but enabled a rapid convergence. Different studies were carried out recently and it was found that LRRA performs better than LRA and NLR if the PSF is symmetric [42, 43]. But NLR is capable of reconstructing object information convoluted with both symmetric as well as asymmetric PSFs.

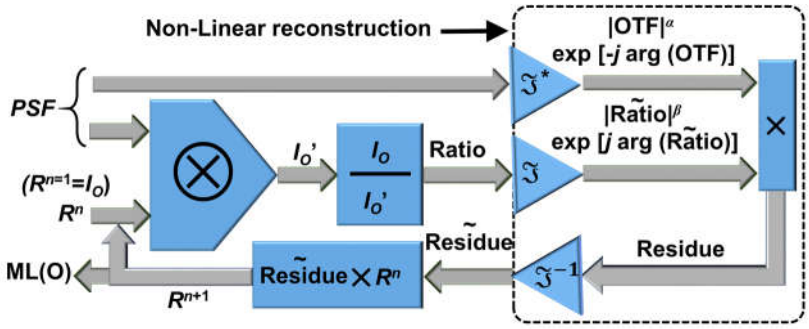

Figure 3. Schematic of the LRRA. The dotted box shows the NLR part of the LRRA.

3. Simulation results

A simulation study was carried out with a matrix size of 500 pixels along x and y directions, pixel size Δ = 10 μm, wavelength λ = 0.65 μm, object distance $z_s = \infty$ and focal length of lens f and distance between lens and sensor z_h are set to the same value $z_s = f$ = 10 cm in MATLAB. Optical configurations with symmetric and asymmetric PSFs were designed. To obtain a symmetric and asymmetric PSF, LADISA with four and three equally spaced sub-apertures were designed respectively. The PSF and MTF given as $|\Im(I_{PSF})|$ of three cases– ideal diffractive lens, one sub-aperture diffractive lens and LADISA for the symmetric case with four sub-apertures are compared in Figure 4. Unlike direct imaging systems where the PSF is the image of a point formed by the imaging device, the PSF is the reconstructed image of a point which is the autocorrelation function. The phase image of an ideal lens, its PSF and MTF are shown in Figures 4(a)-4(c) respectively. The phase image of a sub-aperture diffractive lens, its PSF and MTF are shown in Figures 4(d)-4(f) respectively. The phase image of LADISA, its PSF, autocorrelation using NLR, corresponding MTF, autocorrelation using LRRA and its

Preprints (www.preprints.org) | NOT PEER-REVIEWED | Posted: 15 November 2022 doi:10.20944/preprints202211.0281.v1

corresponding MTF are shown in Figures 4(g)-4(l) respectively. The MTF of LRRA is broader than NLR indicating that higher spatial frequencies are present in the case of LRRA.

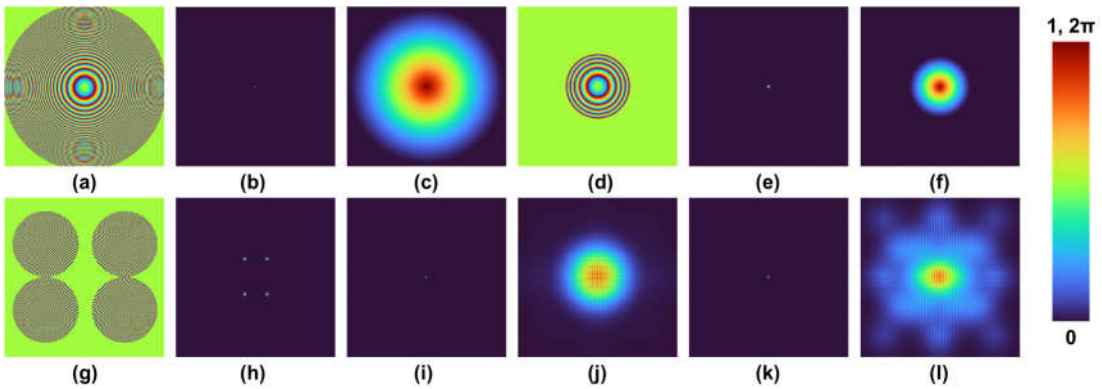

Figure 4. (a) Phase image of ideal diffractive lens, its (b) PSF and (c) MTF. (d) Phase image of a sub-aperture diffractive lens, its (e) PSF and (f) MTF. (g) Phase image of LADISA with four apertures, its' (h) PSF, (i) autocorrelation obtained using NLR and its (j) MTF, (k) autocorrelation obtained using LRRA and its (l) MTF.

A test object 'Emblem of Tartu University' was used for the further simulation studies as shown in Figure 5(a). The imaging results using ideal diffractive lens, sub-aperture diffractive lens, LADISA with four apertures are shown in Figures 5(b)-5(d) respectively. The reconstruction results of the object using NLR and LRRA are shown in Figures 5(e) and 5(f) respectively. The magnified versions of the direct images formed by ideal diffractive lens, sub-aperture diffractive lens, reconstruction results of NLR ($\alpha = 0$, $\beta = 0.6$) and LRRA ($\alpha = 0$, $\beta = 1$, iterations = 15) are shown in Figures 5(g)-5(j) respectively. The above comparison shows the improved resolution with NLR and LRRA and LRRA exhibited a better performance in comparison to both sub-aperture diffractive lens as well as NLR. However, when the PSF is not symmetric such as the case in this study where instead of four sub-apertures if there are only three, then the performances of LRRA is significantly different. The phase image of LADISA with three sub-apertures, its PSF and imaging result of the test object are shown in Figures 6(a)-6(c) respectively. The reconstruction result of NLR ($\alpha = 0$, $\beta = 0.6$) and LRRA ($\alpha = 0$, $\beta = 1$, iterations = 15) are shown in Figures 6(d) and 6(e) respectively. It can be seen that in this case NLR performs better than LRRA. To solve this problem, the PSF and the object intensity distributions were flipped and added with the original images to make them symmetric. The images of the PSF and reconstruction results from LRRA after this process are shown in Figures 6(f) and 6(g) respectively. As it is seen, the reconstruction results significantly improved but the field of view is diminished.

Preprints (www.preprints.org) | NOT PEER-REVIEWED | Posted: 15 November 2022 doi:10.20944/preprints202211.0281.v1

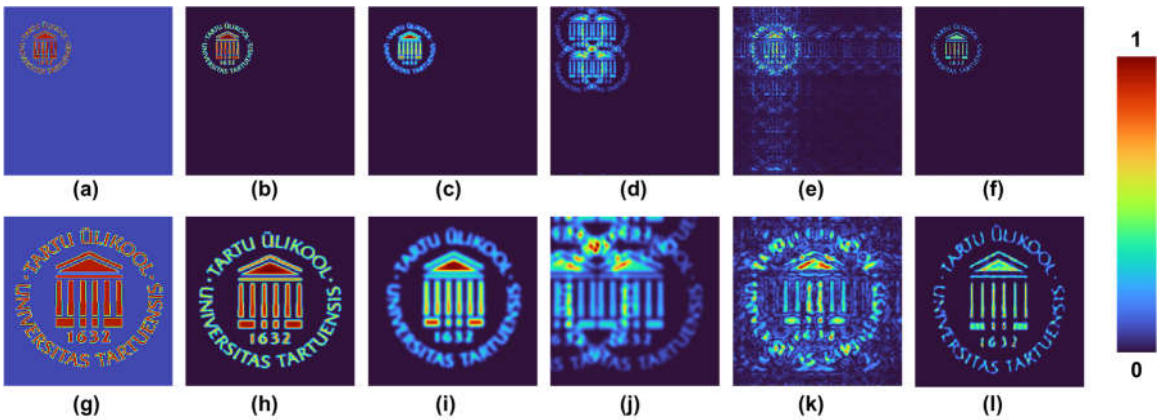

Figure 5. (a) Test object, imaging result from (b) ideal diffractive lens, (c) sub-aperture diffractive lens, (d) LADISA. Reconstruction results of LADISA using (e) NLR and (f) LRRA. The magnified versions of the test object in (a)-(f) are shown in (g)-(l).

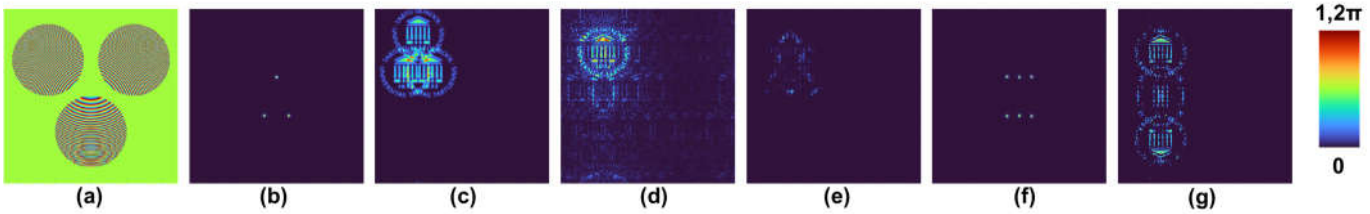

Figure 6. (a) Phase image of LADISA with three sub-apertures (b) PSF, (c) object intensity distribution of the test object. Reconstruction results of LADISA using (d) NLR and (e) LRRA. Image of (f) PSF and (g) reconstruction result from LRRA after post processing by converting the asymmetric distributions into symmetric ones.

4. Fabrication results

The fabrication of LADISA was carried out using photolithography in the ISO5 cleanroom. Positive photoresist (AR-P 3510T, Allresist, Germany) was spin coated (4000 rpm, 60 s) on the top of cleaned ITO (Indium Tin Oxide) coated glass substrates and softly baked on a hot plate at 100 °C for 60 s. The promoter AR 300-80 new (Allresist, Germany) was used to improve the adhesion between the photoresist and the ITO glass. Maskless Aligner (Heidelberg Instruments μMLA 100, Germany) with the dose control of the light source at 390 nm was used to expose the photoresist and an AR 300-44 (Allresist. Germany) was used for developing the UV irradiated structures. Finally, the LADISA were rinsed with ultrapure water to remove possible residuals. The design and the optical microscope ((Nikon Eclipse LV150) image of a section of one of the sub-aperture diffractive lens are shown in Figure 7(a) and 7(b) respectively. The sample was coated with a thin layer (~14 nm) of Au by using direct-current magnetron sputtering and observed under a scanning electron microscope (SEM) FEI Helios NanoLab 600 (FEI, Hillsboro, OR, USA). The SEM image is shown in Figure 7(c). The image of the design is shown in Figure 7(d) and the optical microscope image of a section of one of the sub-apertures of the fabricated element is shown in Figure 7(e).

Preprints (www.preprints.org) | NOT PEER-REVIEWED | Posted: 15 November 2022 doi:10.20944/preprints202211.0281.v1

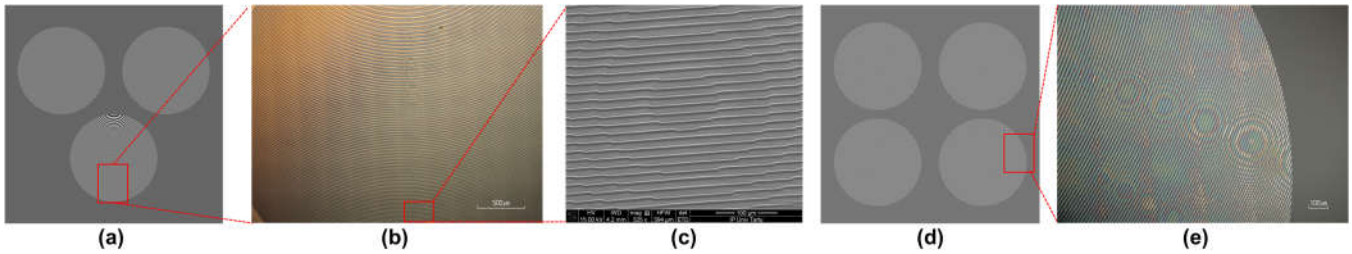

Figure 7. (a) Image of the design of LADISA with three apertures, (b) optical microscope and (c) SEM image of a section of one of the sub-apertures of LADISA, (d) image of the design of LADISA with four apertures and (e) optical microscope image of a section of one of the sub-apertures of LADISA. .

5. Experimental results

The experimental setup used in this study is given in Figure 8. The setup consists of a spatially incoherent high-power LED source (Thorlabs, 170 mW, λ=650 nm and $\Delta\lambda$ = 20 nm). An iris was placed in front of the light source to control light illumination area. A negative USAF test object (Thorlabs) was used for the study. Numeral 2 of size 0.12 × 0.11 mm^2 was critically illuminated by the light source using a refractive lens L1 of focal length 50 mm. The light from the object was collimated by another refractive lens L2 of focal length 80 mm to create large distance effect. This was then collected on an image sensor (Zelux CS165MU/M 1.6 MP monochrome CMOS camera, 1440 × 1080 pixels with pixel size < 3.5 μm) after modulation by the LADISA with the focal length 100 mm. The experiment was carried for two different LADISA apertures, triple and four, and compared with a single aperture. The obtained object intensities (I_O), synthesized PSFs and the corresponding reconstructed images are given in Figure 9.

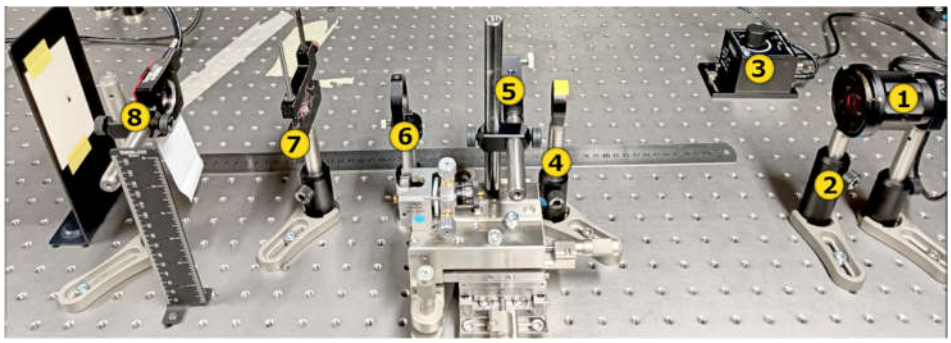

Figure 8. Photograph of the experimental setup: (1) LED, (2) Iris, (3) LED power source, (4) Lens L1 (f = 50 mm), (5) Test object, (6) Lens L2 (f = 35 mm), (7) LADISA, (8) Image sensor.

For the reconstruction, the PSF's are synthesized directly from the recorded images. For this purpose, different point like sharp edges were chosen and the best among them were used for the final reconstruction. The reconstruction parameters for LADISA with triple and four apertures are NLR (α = 0 and β = 0.7) and LRRA (α = 0 and β = 0.9 with 4 iterations). With the addition of more sub-apertures, it is possible to get sharper images. In both cases, LRRA performs better than the NLR. But in the case of three aperture LADISA, the PSF has to be inverted to perform reconstruction in the case of LRRA and with this modification, it can be seen that the results of LRRA was better than NLR. Additional apertures improve the resolution and it can be seen that with four aperture LADISA, LRRA produces sharp images than the single and triple apertures.

Preprints (www.preprints.org) | NOT PEER-REVIEWED | Posted: 15 November 2022 doi:10.20944/preprints202211.0281.v1

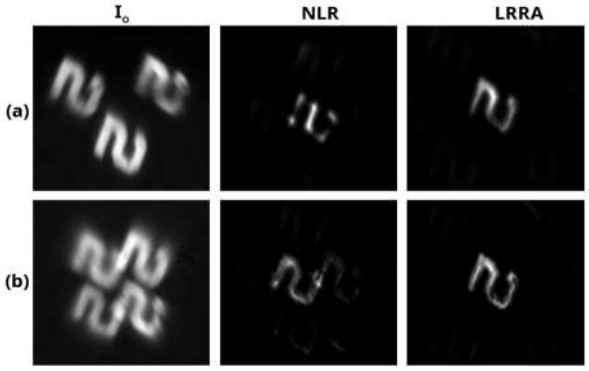

Figure 9. Images of the *Io* of the test object, synthesized PSF and the reconstruction results using NLR and LRRA. (a) and (b) corresponds to the triple and four aperture LADISA.

6. Summary and conclusions

Realization of high resolution in direct imaging systems are often limited by the fabrication capabilities. In the case of diffractive element-based imaging, the outermost zone width of the zone plate is limited to the lithography limit. Secondly, during writing large areas, the beam conditions have to be maintained constant over a long period which is often challenging. Besides the memory size of a single large diffractive lens is significantly high. In this work, we have showed that by adapting Golay-like configuration for the fabrication of diffractive elements and by using indirect imaging principles, it is possible to realize a large area diffractive lens with LADISA. For this purpose, triple and four aperture LADISA elements were designed and their properties were simulated. Since, these apertures are designed in a way to create multifocused image points, the chances of retrieving higher spatial frequencies are improved by manifold. This was shown by the simulation results and in order to further confirm the simulations, triple and four aperture LADISA were fabricated using photolithography and subjected to experimental analysis. It was found that the four aperture LADISA performs better than the three sub-aperture elements in the case of LRRA while NLR showed a similar performance throughout. In the case of symmetric PSFs, LRRA always perform better than NLR. Since, spatial aberration correction has already been shown in the case of a refractive lens in which LRRA performed better than NLR, we believe that the spatial and spectral aberrations associated with diffractive lens can be corrected with LRRA [42]. We believe these results can be implemented to manufacture portable, low-weight devices with higher resolution, such as telescopes, lensless cameras and microscopes.

Author Contributions: Conceptualization, V. A.; methodology, V. A., A. T., S. J. and K. K; software, S.G., P. P. A., T. K. and V. A; validation, S.G., A. B., P. P. A., T. K., A. T., K. K., S. H. N., D. S., F. G. A. and V. A.; formal analysis, V. A., A. T. and K. K; investigation, S.G., A. B., P. P. A., T. K.; resources, A.T., K. K. and V. A.; fabrication of LADISA, T. K., A. T., and K. K.; SEM characterization of LADISA, T. K., A. T., and K. K.; data curation, S.G., P. P. A. and T. K.; writing—original draft preparation, V. A., T. K., P. P. A. and S. G.; writing—review and editing, all the authors.; visualization, V. A., T. K., P. P. A and S. G.; supervision, V. A., A. T., S. J. and K. K.; project administration, V. A., A. T., S. J. ; funding acquisition, V. A., A. T., S. J. . All authors have read and agreed to the published version of the manuscript.

Funding: This research was funded by European Union's Horizon 2020 research and innovation programme grant agreement No. 857627 (CIPHR) and ARC Linkage LP190100505 project. The present study was partially funded by the European Regional Development Fund project "Emerging orders in quantum and nanomaterials" (TK134) and Estonian Research Agency (PRG4).

Acknowledgments: The authors thank Aravind Simon and Tiia Lillemaa for their administrative support, Helle-Mai Piirsoo for SEM measurements and Peeter Ritslaid for magnetron sputtering. This work were acknowledging the ERDF project Centre of Technologies and Investigations of Nanomaterials (NAMUR+, project number 2014-2020.4.01.16-0123) and the NAMUR+ core facility funded project by the Estonian Research Council (TT 13).

Conflicts of Interest: The authors declare no conflict of interest.

References

1. Bhandari, A.; Kadambi, A.; and Raskar, R. Computational Imaging. *MIT Press.* **2022**.
2. Javidi, B.; Carnicer, A.; Anand, A.; Barbastathis, G.; Chen, W.; Ferraro, P.; Goodman, J.W.; Horisaki, R.; Khare, K.; Kujawinska, M.; and Leitgeb, R.A. Roadmap on digital holography. *Opt.Express*. **2021**, 29, 35078-35118.
3. Thomas Cathey, W.; and Dowski, E. R. New paradigm for imaging systems. *Appl. Opt.* ***2002***, 41, 6080-6092.
4. Tahara, T.; Zhang, Y.; Rosen, J.; Anand, V.; Cao, L.; Wu, J.; Koujin, T.; Matsuda, A.; Ishii, A.; Kozawa, Y.; and Okamoto, R. Roadmap of incoherent digital holography. *Appl. Phys.B.* **2022**, 128(11), pp.1-31.
5. Rosen, J.; Vijayakumar, A.; Kumar, M.; Rai, M.R.; Kelner, R.; Kashter, Y.; Bulbul, A.; and Mukherjee, S. Recent advances in self-interference incoherent digital holography. *Adv. Opt. Photonics.* **2019**, 11(1), pp.1-66.
6. Murty, M. V. R. K.; and Hagerott, E. C. Rotational shearing interferometry. *Appl. Opt*. **1966,** 5, 615–619.
7. Armitage, J. D.; and Lohmann, A. Rotary shearing interferometry. *Opt. Acta*. **1965**, 12, 185–192.
8. Shaked, N. T.; Katz, B.; and Rosen, J. Review of three-dimensional holographic imaging by multiple-viewpoint-projection based methods. *Appl. Opt*. **2009**, 48, H120–H136.
9. Rivenson, Y.; Stern, A.; and Rosen, J. Compressive multiple view projection incoherent holography. *Opt. Express*. **2011**, 19, 6109–6118.
10. Sirat, G. Y. Conoscopic holography. I. Basic principles and physical basis. *J. Opt. Soc. Am. A.* **1992**, 9, 70–83.
11. Mugnier, L. M.; and Sirat, G. Y. On-axis conoscopic holography without a conjugate image. *Opt. Lett.* **1992,** 17, 294–296.
12. Schilling, B.W.; Poon, T. C.; Indebetouw, G.; Storrie, B.; Shinoda, K.; Suzuki, Y.; and Wu, M. H. Three-dimensional holographic fluorescence microscopy. *Opt. Lett*. **1997**, 22, 1506–1508.
13. Poon, T. C.; and Indebetouw, G. Three-dimensional point spread functions of an optical heterodyne scanning image processor. *Appl. Opt*. **2003**, 42, 1485–1492 .
14. Rosen, J.; and Brooker, G. Digital spatially incoherent Fresnel holography. *Opt. Lett*. **2007**, 32, 912-914.
15. Rosen, J.; and Brooker, G. Non-scanning motionless fluorescence three-dimensional holographic microscopy. *Nat. Photon*. **2008**, 2(3), pp.190-195.
16. Vijayakumar, A.; Kashter, Y.; Kelner, R.; and Rosen, J. Coded aperture correlation holography—a new type of incoherent digital holograms. *Opt. Express.* **2016,** 24, 12430–12441.
17. Ables, J. G. Fourier transform photography: a new method for X-ray astronomy. *Proc. Astron. Soc. Aust*. **1968**, 1, 172–173.
18. Dicke, R.H. Scatter-hole cameras for X-rays and gamma rays. *Astrophys. J.* **1968**, 153, L101.
19. Fenimore, E. E.; and Cannon, T. M. Coded aperture imaging with uniformly redundant arrays. *Appl. Opt*. **1978**, 17, 337-347.
20. Tsai, TH.; and Brady, D. J. Coded aperture snapshot spectral polarization imaging. *Appl. Opt*. **2013**, 52, 2153-2161.
21. Sahoo, S.K.; Tang, D.; and Dang, C. Single-shot multispectral imaging with a monochromatic camera. *Optica*. **2017**, *4*, 1209-1213.
22. Vijayakumar, A.; and Rosen, J. Interferenceless coded aperture correlation holography–a new technique for recording incoherent digital holograms without two-wave interference. *Opt. Express*. **2017**, 25, 13883-13896.
23. Antipa, N.; Kuo, G.; Heckel, R.; Mildenhall, B.; Bostan, E.; Ng, R.; and Waller, L. DiffuserCam: lensless single-exposure 3D imaging. *Optica*. **2018**, *5*, 1-9.
24. Anand, V.; Ng, S.H., Maksimovic, J. et al. Single shot multispectral multidimensional imaging using chaotic waves. *Sci Rep*, **2020**, 10, 13902.
25. Golay, M. Point arrays having compact non-redundant autocorrelations. *J. Opt. Soc. Am*. **1971**, 61, 272–273.
26. Meinel A. B.; and Meinel, M. P. Large sparse-aperture space optical systems. *Opt. Eng.* **2002**, 41, 1983–1994.
27. Miller, N. J.; Dierking, M. P.; and Duncan, B. D. Optical sparse aperture imaging. *Appl. Opt.* **2007**, 46, 5933-5943.
28. Vijayakumar, A.; Jayavel, D.; Muthaiah, M.; Bhattacharya, S.; and Rosen, J. Implementation of a speckle-correlation-based optical lever with extended dynamic range. *Appl. Opt*. **2019**, 58, 5982-5988.
29. Paykin, I.; Yacobi, L.; Adler, J.; and Ribak, E. N. Phasing a segmented telescope. *Phys. Rev. E.* **2015**, 91(2), 023302.
30. Ding, J.; Noshad, M.; and Tarokh, V. Complementary lattice arrays for coded aperture imaging. *J. Opt. Soc. Am. A*. **2016**, 33, 863-881.
31. Vijayakumar, A.; and Bhattacharya, S. Design and Fabrication of Diffractive Optical Elements with MATLAB. *SPIE.* **2017**.
32. Meem, M.; Banerji, S.; Pies, C.; Oberbiermann, T.; Majumder, A.; Sensale-Rodriguez, B.; and Menon, R. Large-area, high-numerical-aperture multi-level diffractive lens via inverse design. *Optica.* **2020**, 7, 252-253.
33. Wang, L.; Xu, B.B.; Cao, X.W.; Li, Q.K.; Tian, W.J.; Chen, Q.D.; Juodkazis, S.; and Sun, H.B. Competition between subwavelength and deep-subwavelength structures ablated by ultrashort laser pulses. *Optica.* **2017**, 4(6), pp.637-642.
34. Kress, B.C.; and Meyrueis, P. Applied digital optics: from micro-optics to nanophotonics. *John Wiley & Sons.***2014**.
35. Vijayakumar, A.; and Bhattacharya, S. Characterization and correction of spherical aberration due to glass substrate in the design and fabrication of Fresnel zone lenses. *Appl. Opt*. **2013**, 52, 5932-5940.
36. Horner, J.L.; Gianino, P.D. Phase-only matched filtering. Appl. Opt. **1984**, 23, 812–816.
37. Khireddine, A.; Benmahammed, K.; Puech, W. Digital image restoration by Wiener filter in 2D case. *Adv. Eng. Software* **2007**, 38, 513–516.
38. Rai, M.R.; Anand, V.; Rosen, J. Non-linear adaptive three-dimensional imaging with interferenceless coded aperture correlation holography (I-COACH). *Opt. Express* **2018**, 26, 18143–18154.

39. Richardson, W.H. Bayesian-Based Iterative Method of Image Restoration. *J. Opt. Soc. Am*. **1972**, 62, 55–59.
40. Lucy, L.B. An iterative technique for the rectification of observed distributions. *Astron. J*. **1974**, 79, 745.
41. Anand, V.; Han, M.; Maksimovic, J.; Ng, S.H.; Katkus, T.; Klein, A.; Bambery, K.; Tobin, M.J.; Vongsvivut, J.; Juodkazis, S.; et al. Single-shot mid-infrared incoherent holography using Lucy-Richardson-Rosen algorithm. *Opto-Electron. Sci.* **2022**, *1*, 210006.
42. Praveen, P.A.; Arockiaraj, F.G.; Gopinath, S.; Smith, D.; Kahro, T.; Valdma, S.-M.; Bleahu, A.; Ng, S.H.; Reddy, A.N.K.; Katkus, T.; Rajeswary, A.S.J.F.; Ganeev, R.A.; Pikker, S.; Kukli, K.; Tamm, A.; Juodkazis, S.; Anand, V. Deep Deconvolution of Object Information Modulated by a Refractive Lens Using Lucy-Richardson-Rosen Algorithm. *Photonics* **2022**, *9*, 625.
43. Anand, V.; Khonina, S.; Kumar, R.; Dubey, N.; Reddy, A.N.K.; Rosen, J.; Juodkazis, S. Three-dimensional incoherent imaging using spiral rotating point spread functions created by double-helix beams. *Nanoscale Res. Lett*. **2022**, 17, 1–13.
44. Smith, D.; Gopinath, S.; Arockiaraj, F.G.; Reddy, A.N.K.; Balasubramani, V.; Kumar, R.; Dubey, N.; Ng, S.H.; Katkus, T.; Selva, S.J.; Renganathan, D.; Kamalam, M.B.R.; John Francis Rajeswary, A.S.; Navaneethakrishnan, S.; Inbanathan, S.R.; Valdma, S.-M.; Praveen, P.A.; Amudhavel, J.; Kumar, M.; Ganeev, R.A.; Magistretti, P.J.; Depeursinge, C.; Juodkazis, S.; Rosen, J.; Anand, V. Nonlinear Reconstruction of Images from Patterns Generated by Deterministic or Random Optical Masks—Concepts and Review of Research. *J. Imaging* **2022**, *8*, 174.